Assessing the dephasing dynamics of water from linear field-resolved pulse propagation experiments and simulations in highly absorbing solutions

Julie A. Gruetzmacher,[a),b)] Rene A. Nome,[a),c)] Andrew M. Moran,[d)] and Norbert F. Scherer[e)]
Department of Chemistry, The James Franck Institute, The University of Chicago,
Chicago, Illinois 60637, USA

We measure and simulate electric field distortions resulting from propagation of mid-infrared pulses that are resonant with the OH stretch vibration through optically dense HDO:D_2O. These distortions are characterized experimentally by full-field-resolved time- and frequency-domain measurements, specifically cross-correlation frequency-resolved optical gating and spectral interferometry, establishing amplitude and phase of the signal fields. Correlation-function finite-difference time-domain (CF-FDTD) simulations using response functions for the OH-stretching vibration, obtained from nonlinear spectroscopic studies reported by others, show that details of the line shape functions are manifested in the measured (linear-response) spectrograms. The degree of homogeneous or inhomogeneous broadening present in the various model correlation functions is readily apparent in the measured and simulated signals. Surprisingly, the published correlation functions are shown to range from modest inhomogeneous to homogeneous line broadening. The present experimental and simulation approach is very useful for establishing the correct form of energy gap correlation functions and dephasing dynamics of IR and optical transitions. In the case of HDO:D_2O, correlation functions with modest inhomogeneous broadening better reflect our measured responses. © *2008 American Institute of Physics.* [DOI: 10.1063/1.2990654]

I. INTRODUCTION

The application of ultrashort pulses to problems in femtosecond spectroscopy increasingly relies on robust and sensitive methods of signal detection. Knowledge of the amplitude and phase of the signal field in linear or nonlinear spectroscopy allows extracting aspects of the real and imaginary components of the refractive index (or susceptibility or response function) of a given material under investigation.[1] Consequently, the electric field is the quantity that recently developed pulse characterization techniques strive to measure.[2–13]

A simple experiment that highlights the importance of full-field characterization of spectroscopic signals is linear spectroscopic measurement of femtosecond pulses propagating through optically dense materials.[13] For a material consisting of noninteracting absorbers, absorption is usually expressed in terms of Beer's law for the steady-state condition of conventional linear spectroscopy. On the other hand, pulse distortion effects have been observed for the resonant propagation of finite bandwidth pulses in/through such systems.[14–16] This problem has been investigated for various waveforms.[17]

Pulse-shape distortion has characteristics that are best described in the frequency or time domain. The Fourier components of the pulse that lie near the center of the resonance are attenuated more than those in the spectral wings. Furthermore, the output pulse is primarily formed from the field components in the leading edge of the input pulse and less so from components at the temporal peak of the input pulse.[18] Also, the signal emission time, or the instant the peak of the pulse emerges from the sample, is given by the classical group velocity expression $c/[n+v(dn/dv)]$. These conclusions are related to each other by the Fourier-transform shift theorem that relates a linear term in the spectral phase to a shift in the signal emission time.[19]

Garrett and McCumber first investigated resonant propagation of weak Gaussian-shaped pulses with durations much longer than the dephasing time.[18] This limit is relevant to studies involving femtosecond pulses that are resonant with electronic transitions in the visible and near-infrared spectral ranges, where the pulse bandwidth is typically (much) smaller than the absorption line. In this limit, the Taylor series expansion of the spectral phase $\varphi(\omega)$,

$$\varphi(\omega) = \varphi(\omega_0) + (\omega - \omega_0)\frac{d\varphi}{d\omega} + \tfrac{1}{2}(\omega - \omega_0)^2\frac{d^2\varphi}{d\omega^2} + \cdots,$$

(1)

converges, and the spectral phase across the pulse bandwidth is nearly linearly dependent on frequency. Therefore, techniques commonly used for dispersive pulse propagation can be extended to investigate anomalous dispersion.[18] This

---

a)These two authors contributed equally to this work.
b)Current address: Nuclear Engineering Division, Argonne National Laboratory, Argonne, Illinois 60439, USA.
c)Current address: Center for Nanoscale Materials, Argonne National Laboratory, Argonne, Illinois 60439, USA.
d)Current address: Department of Chemistry, University of North Carolina at Chapel Hill, North Carolina 27599, USA.
e)Electronic mail: nfschere@uchicago.edu.

analysis is useful for the study of propagation of pulses with narrow bandwidth (compared to the material linewidth) and for small propagation distances through samples with low optical density. Otherwise, the spectrum becomes sufficiently distorted that the concept of a dominant central frequency eventually fails, and the classical group velocity expression no longer applies.[17]

Another commonly encountered limit occurs when the pulse spectrum is comparable to or broader than the absorption line of the medium of interest. Linear measurements of resonant pulse propagation in the mid-infrared spectral region have shown that signal profiles can undergo significant distortions when the pulse duration is shorter than the material dephasing times.[14–16] The consequence in, for example, nonlinear optical experiments would be the continuing evolution (distortion) of the driving (applied) fields that create the nonlinear polarization in the medium as well as the concomitant distortions of the signal field resulting from integration of this polarization over the interaction length with the material.

We developed the correlation-function-based finite-difference time-domain (CF-FDTD) method to simulate pulse propagation without invoking standard approximations (i.e., slowly varying envelope, rotating wave, and Markovian material response).[13,20] This computational technique incorporates the energy gap fluctuation correlation function[1] of a two-level system to describe the (potentially) non-Markovian medium response. It is also a first step toward similar modeling of nonlinear responses. Since the CF-FDTD method can incorporate any sum of correlation functions and the field profiles are sensitive to rapid dephasing dynamics, the description of relaxation by a given correlation function can be examined by comparing CF-FDTD simulation results with experimentally determined electric fields.

The present paper introduces a combined experimental-computational strategy for examining correlation-function descriptions of fast relaxation dynamics and is applied to ultrafast infrared pulse propagation in liquid water. The method entails electric field (amplitude- and phase-) sensitive measurements of (vibrationally) resonant pulses that have propagated through a highly absorptive sample with full-field pulse propagation simulations. The CF-FDTD method is used to examine correlation functions for the OH-stretching vibration of HDO in D_2O obtained from recently reported mid-IR pump-probe and photon echo experiments.[21–24] Even though these correlation functions should have been constrained to fit to the linear absorption spectrum of the OH-stretching vibration, we find that they range from modest inhomogeneous to homogeneous line broadening regimes. This finding suggests that a simple and robust diagnostic for complete determination of dephasing dynamics is required to address otherwise indeterminate cases. The determination of pulse distortions in highly absorptive samples and the CF-FDTD analysis described here provides useful constraints. Specifically, the present paper shows that this experimental and simulation approach can readily distinguish homogeneous from inhomogeneous line
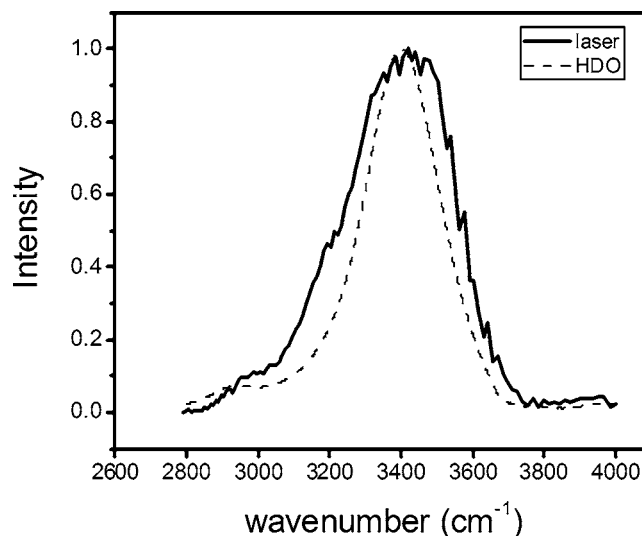

FIG. 1. Mid-IR absorption spectrum of HDO:D_2O (1:50; black curve) and laser pulse (dashed curve).

broadening dynamics at the level of linear spectroscopy and readily distinguishes between the various correlation functions previously proposed for HDO.

II. EXPERIMENTAL FIELD DETERMINATION

The mid-IR femtosecond pulse source was a home-built Ti:sapphire system (cavity-dumped oscillator, chirped pulse regenerative amplifier) followed by a double-pass $KNbO_3$ (KN) mid-infrared optical parametric amplifier.[28] The laser system described in reference 28 has been substantially improved in power output for the spectral interferometry measurements.[25] Using a 5.5 mJ/pulse 532 nm pump, an amplifier with longer radius of curvature mirrors ($R = 50$ cm) and translating the Ti:S crystal by ~1 cm from the focus toward the converging pump beam gives 500 μJ pulses of ~50 fs duration. The pulse energy from the double-passed KN OPA is ~100 nJ. Ultrashort mid-IR pulses (75 fs at 3 μm), resonant with the OH-stretching mode of HDO in D_2O, propagated through 200 μm thick samples with different optical densities at the absorption maximum (O.D. 1.7, 0.9, and 0.5, corresponding to molar ratios of 1/50, 1/100, and 1/200 HDO:D_2O; see Fig. 1). These concentrations are close to those used in Refs. 21–24 thereby allowing a direct comparative study and also a treatment of the O–H stretching modes as individual oscillators.[26,27] Pulse profiles before and after the samples were characterized by cross-correlation frequency-resolved optical gating[19] (XFROG) (with a 42 fs, 800 nm gate pulse) and by spectral interferometry. The XFROG spectrograms were analyzed with commercial software (FROG 3.06, Femtosoft Technologies) to extract the amplitudes and phases of the pulse electric fields. While the XFROG method is typically used for pulse characterization, it has also been utilized to determine the electric field of molecular signals.[28–30] In the spectral interferometry measurements, the OPA output was sent to a Mach–Zender interferometer with a delay such that the reference pulse preceded the signal by a fixed time delay. The unknown signal was generated by placing the

sample in one arm of the interferometer. A microstepping motorized linear stage (Melles Griot) was used for precise determination of the time delay between pulses, and a pair of calcium fluoride beam splitters (Alpine Research Optics) were used to split the mid-infrared pulses. The reference and signal beams were imaged into a spectrometer (TRIAX 320, Jobin-Yvon) connected to a HgCdTe array with 6 nm/pixel resolution (IR 6416, Infrared Systems). Spectra were acquired using a grating blazed at 2500 nm (120 groove/mm). Successive spectral interferograms indicated negligible path-length drift over 30 min.

III. COMPUTATIONAL METHOD

Full-field-resolved simulations of ultrafast pulse propagation were performed using the CF-FDTD method for solving Maxwell's equations.[13,20,31,32] In this formalism, population relaxation is described phenomenologically as an exponential decay with rate constant equal to $1/T_1$, and the system-bath interaction is captured using a correlation-function description of relaxation. As shown in Ref. 13, the line shape function, $g(t) = \int_0^t d\tau_2 \int_0^{\tau_2} d\tau_1 C(\tau_1)$, is incorporated into the relaxation term of the Liouville equation,[1] leading to the Maxwell–Liouville CF-FDTD equations. The equation of motion of the density matrix for a real line shape function is

$$
\frac{\partial}{\partial t}\begin{pmatrix} \rho_1 \\ \rho_2 \\ \rho_3 \end{pmatrix} = \begin{pmatrix} 0 & \omega_0 & 0 \\ \omega_0 & 0 & 2\frac{\mu}{\hbar}E_x \\ 0 & 2\frac{\mu}{\hbar}E_x & 0 \end{pmatrix}\begin{pmatrix} \rho_1 \\ \rho_2 \\ \rho_3 \end{pmatrix}
$$
$$
+ \begin{pmatrix} \dot{g}(t) & 0 & 0 \\ 0 & \dot{g}(t) & 0 \\ 0 & 0 & \frac{1}{T_1} \end{pmatrix}\begin{pmatrix} \rho_1 \\ \rho_2 \\ \rho_3 - \rho_{30} \end{pmatrix}, \quad (2)
$$

where ρ_1 and ρ_2 are the in-phase (additive) and out-of-phase (subtractive) "off-diagonal" matrix components; ω_0 is the transition frequency, μ is the transition dipole moment, T_1 is the population relaxation time, ρ_3 is the population difference between excited and ground states, and ρ_{30} is the initial inversion; the overdot indicates the first derivative with respect to time. E_x is the x-polarized electric field calculated in the one-dimensional CF-FDTD simulation (propagation along z). This leads to a set of coupled Maxwell–Liouville equations for subsequent finite differencing. A detailed description of the algorithm is given in Ref. 13. Appendix A expands this equation to a cascaded three-level system as needed for nonlinear spectroscopies.

The basic quantities required for the simulation are estimated from a combination of literature values and experimentally determined parameters. The number density and path length given in Table I are pertinent to our experiment. The transition dipole moment is estimated from the integrated area of the absorption band[33] via the Einstein B coefficient for absorption. The permittivity of the medium is taken as that of neat D_2O at the carrier frequency of the pulse, as determined by attenuated total reflectance Fourier-

TABLE I. Parameter values for simulations.

Parameter	Value
N (number density)	1.66×10^{26} m^{-3} to 6.66×10^{26} m^{-3}
Path length	2.0×10^{-4} m
Initial pulse duration (FWHM)	88.0×10^{-15} s
Pulse chirp	4.4×10^{25} rad s^{-2}
Carrier frequency	6.412×10^{12} rad s^{-2}
Dipole moment μ	7.612×10^{-31} C m
Dielectric permittivity of D_2O, ε_{D_2O}	1.457×10^{-11} J^{-1} C^2 m^{-1}

transform infrared spectroscopy.[34] The initial pulse parameters for our measurements are obtained from XFROG measurements of the instrument response. The pulse chirp is determined by a polynomial fit to the temporal phase extracted by the XFROG (or spectral interferometry) analysis and is included in the simulation to second order; third and higher order phase terms did not significantly modify the results and, hence, are not included in the results shown here. The dispersion of the solvent is not included in the simulation, which only deals with resonant chromophore-field interactions in its current form.[13] The window dimensions (two windows each 1 mm thick) are too large to incorporate into the calculation while maintaining a reasonable computation time. Therefore, an 88 fs (FWHM Gaussian) "pre-broadened" initial pulse duration is used to account for pulse spreading due to propagation through the D_2O solvent and the CaF$_2$ sample cell windows. The values of the constants used in the simulations are provided in Table I. Given that the CF-FDTD formalism requires the line shape function $g(t)$ to be evaluated at every iteration (i.e., at each time step of the coupled Maxwell–Liouville equations solved by FDTD), $g(t)$ must only evolve once the field (pulse) interacts with the sample. For simplicity, $g(t)$ is set to zero before the peak of the pulse arrives at the sample and the evolution of $g(t)$ begins when the peak of the pulse arrives at the beginning of the sample (in practice, the field has propagated for 400 fs to this point).

IV. RESULTS

A. Time-frequency-domain perspective

Previous measurements of pulse profiles after propagation through solutions of HDO in liquid D_2O with concentrations commonly used in nonlinear studies have observed beat-like distortions of the incident fields at high optical densities.[28,29] Figure 2 displays the spectrogram and calculated field characteristics of a pulse after traversing the most optically dense (i.e., 1/50 HDO:D_2O) sample, which will be used as the point of comparison for the simulation results. The intensity profile shows a beat-like structure, and a phase jump of approximately π radians at the location of the first minimum of the intensity profile. An apparent pulse compression is observed as the incoming pulse decays more rapidly at high optical density: a Gaussian fit to the first peak of the intensity profile (at $\sim$ time zero in Fig. 2), which is associated with the incoming field, reveals that it decreases from 88 fs in the absence of the absorbing solution to 45 fs at an optical density of 1.7 for the 1:50 HDO:D_2O solution.
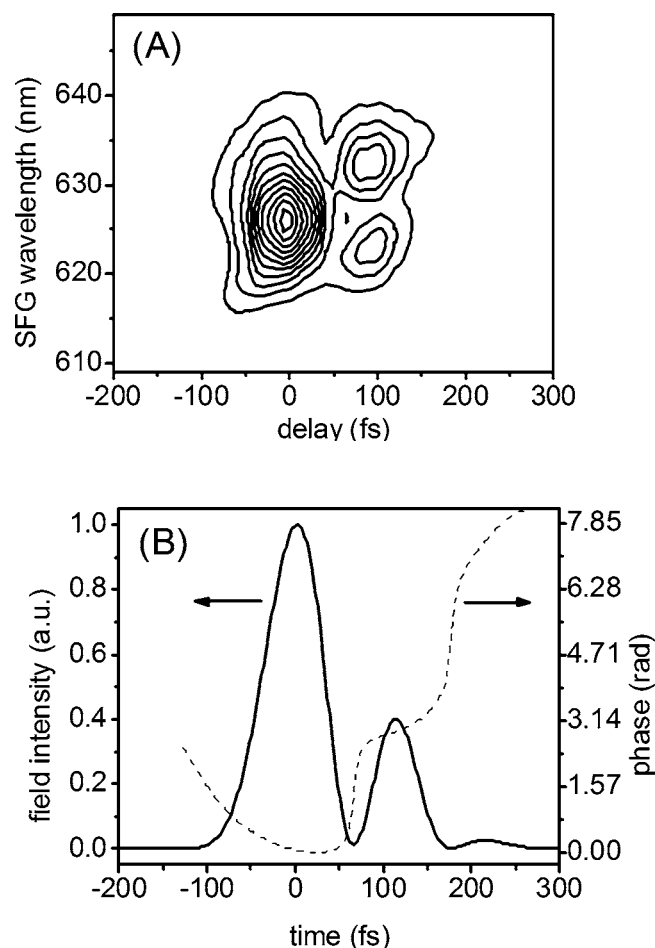
FIG. 2. (a) Experimental XFROG spectrogram of the mid-IR pulse after propagation through a 1:50 HDO:D_2O sample (path length=0.200 mm, OD 1.7). Contours are at 5% levels; (b) Electric field amplitude (intensity) and phase extracted from the spectrogram. Solid line: field intensity; dashed line: phase.

FIG. 3. (Color online) Phase and amplitude vs frequency plots of HDO:D_2O. Black solid line: 1:50 sample; red-dot-dashed curve: 1:100; blue dotted curve: 1:200. Black dashed curve in the lower panel: Fourier transform of the time-domain (XFROG) result (sample: 1:50).

These qualitative experimental observations can be explained by analyzing the dynamics of the driving field and of the polarization in the limit where the pulse duration is similar to the dephasing time scale.[18,35,36] When an ultrashort pulse propagates through an optically dense medium, its leading edge excites a macroscopic polarization in the sample. The emitted field is 180° out of phase with respect to the input pulse for a time of the order of the dephasing time. If the trailing edge of the pulse drops off faster than the decay of the macroscopic polarization, then the temporal envelope of the electric field leaving this medium will go through zero and become negative (phase changes of π in the electric field cause the envelope to change sign). In highly absorbing media this free induction decay can become a new "driving pulse" and spawns a second FID. The resulting multiple FID (i.e., beats) signal originates from a sequence or cascade of responses, i.e., field absorption-polarization evolution-emission cycles.

At first glance the emitted multi-beat waveform appears to be a nonlinear polarization response in which the field-response-field, etc. operations do not commute. However, there are only two field-matter interactions at each spatial location of the sample. After the first field interaction the
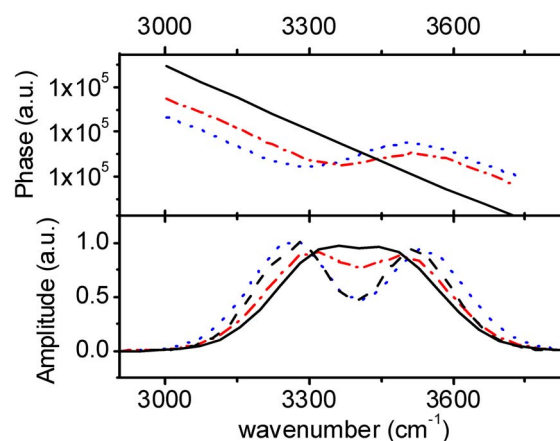
system evolves in accord with the coherence relaxation dynamics associated with the system-bath interaction (i.e., dephasing time). As the fields propagate through the material, the re-radiated field does not interact again with the molecules from which it was emitted and, hence, the spectroscopy is linear.

Spectral amplitude and phase profiles of the propagated fields were also obtained directly using spectral interferometry.[37–39] Figure 3 shows that the experimentally retrieved spectral amplitudes are double peaked and the depth of the spectral hole increases with optical density. This shape is expected as absorption of light by the OH-stretching band removes resonant spectral content from the pulse. These observations are consistent with the time-domain pulse propagation results described above as well as with Fourier transforms of the time-domain electric fields determined by XFROG (see Fig. 3).

The frequency-domain pulse propagation data of Fig. 3 indicates that the absorbing medium attenuates the pulse spectrum at its center. When the pulse duration is shorter than the dephasing time, absorption measured by spectral interferometry has three origins. First, at resonance, coherent destructive interference occurs between incoming and emitted fields at the sample (as revealed by pulse "compression" of the first peak in the temporal intensity profile of Fig. 2). Second, interference also occurs at the exit port of the spectrometer, where temporally separated field envelopes associated with each FID beat, which are π out of phase, are dispersed and thus interfere destructively. Third, small absorption of the Fourier components that are farther off-resonance, for which the phase shift is not π, also contributes to the measured signal. In this way, the pulse spectrum develops a dip and resembles the spectrum obtained from the superposition of two quasimonochromatic waves which differ slightly in central frequency, thus, leading to beats in the time domain. As the concentration increases, more frequency components farther off resonance contribute to the signal. As a result, the two spectral peaks around the center are pushed away from resonance, leading to an increase of the apparent
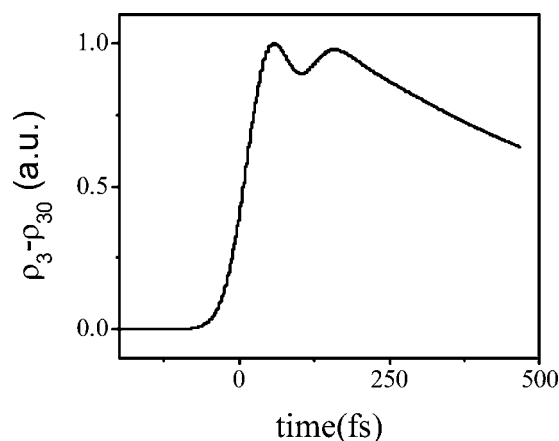
FIG. 4. Normalized excess population versus time. Mole ratio: 1:50 HDO:D_2O. Time-zero indicates the time of arrival of the peak of the pulse at the sample. Spectral amplitudes and phases measured by spectral interferometry as a function of concentration.

FIG. 5. (Color online) Comparison of OH frequency correlation functions taken from the literature. Black solid line: Fecko et al. (Ref. 22); red dashed: Woutersen and Bakker (Ref. 21); green dotted curve: Piryatinski et al. (Ref. 41); blue dot-dashed curve: Stenger et al. (Ref. 23); cyan double dot-dashed: Yeremenko et al. (Ref. 24). See Table II and Appendix B for correlation-function parameters.

frequency of the beats. Thus, the effects of resonant pulse propagation are related to refraction near resonance as well as absorption at resonance.

These complementary time- and frequency-domain perspectives mirror a number of interpretations that have been given to explain the characteristics of FID beats.[14–19] The time-domain description of the phenomena in terms of destructive interference between driving and generated fields treats only resonant interactions; this picture makes intuitive sense when the results of the XFROG analysis are examined, as in Fig. 2(b), and follows the interpretation given in Refs. 14–19. On the other hand, the pulse spectral components towards the wings of the absorption are not absorbed as effectively. These near-resonant contributions to the signal (from the pulse spectral wings) must not be neglected. Note that the relationship between FID phase change and the absorption spectrum, as calculated in Ref. 46, is valid in the limit where the material bandwidth is much larger than the laser bandwidth. This assumption does not hold for ultrashort midIR pulses propagating through HDO/D_2O.

B. Correlation-function FDTD simulations

The CF-FDTD simulations provide further insights into mechanisms of pulse distortion. Figure 4 shows numerical results for the excess population of the first vibrationally excited state, ρ_3-ρ_{30} in Eq. (2), as a function of time. At short times, ρ_3-ρ_{30} rises rapidly with time to a delayed maximum with respect to the driving field. Subsequently, ρ_3-ρ_{30} undergoes an oscillation resulting from the time dependence of the electric field and polarization. For longer times, ρ_3-ρ_{30} decays exponentially with the population lifetime, T_1. The dip at 200 fs results from the coherent interaction of the pulse with the macroscopic excitation of the sample. Similar results were obtained from CF-FDTD simulations of a cascaded three-level system (see Ref. 25 and Appendix A) indicating that the third level is not involved in the present linear spectroscopy measurement. It is important to emphasize that the population change is normalized; the transient response in Fig. 4 does not involve significant population changes of the vibrational states (i.e., the fractional change is less than
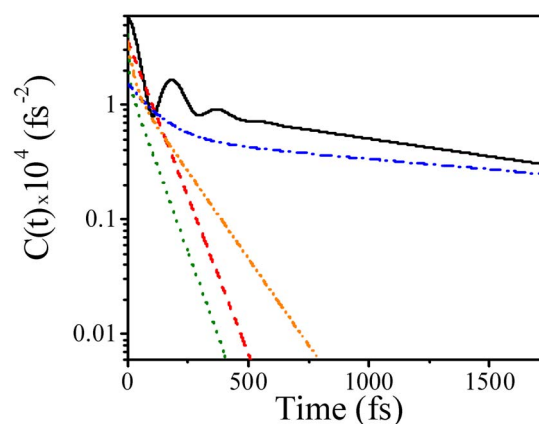
10^{-21}). In contrast, coherent nonlinear phenomena such as self-induced transparency are described by the same equation (2) for intense pulses with considerable population changes.[40]

C. Correlation-function dependence of the propagated fields

The pulse propagation experiment described above is unable to uniquely determine the material response function or correlation function on its own, but exhibits considerable sensitivity to fast dephasing dynamics. Therefore, this measurement is to be used in conjunction with the CF-FDTD simulations as a test bed for correlation functions determined through other measurements or as a constraint on modeling correlation functions. To illustrate, we use models of the response of the OH-stretching vibration obtained from published pump-probe and photon echo studies.[21–24] Energy gap correlation functions constructed to match the relaxation phenomena observed in those measurements are used in the CF-FDTD algorithm to simulate the response of the water sample. The correlation functions in Refs. 21, 23, and 24 have the general form

$$C(\tau) = \Delta_1^2 e^{-\Lambda_1 \tau} + \Delta_2^2 e^{-\Lambda_2 \tau} + \frac{\delta(\tau)}{T_2}, \tag{3}$$

where Λ_i is the inverse correlation time, Δ_i is the root mean squared (rms) amplitude of the frequency fluctuation, T_2 is the dephasing time corresponding to homogeneous (Bloch limit) dephasing, and $\delta(\tau)$ is the delta function. The correlation function from Ref. 22 and the corresponding line shape function $g(t)$ are presented in Appendix B. (For the CF-FDTD simulations, $g(t)$ derived from Ref. 22 was multiplied by 0.6. This was done such that $\int_{-\infty}^{\infty} dt \exp[i(\omega - \omega_0)t - g(t)]$ matches the experimental absorption spectrum, which we felt was an essential constraint; the other three correlation and lineshape functions used give good agreement with the experimental spectrum). Figure 5 shows the correlation functions obtained from the literature[21–24,41] and used in this

TABLE II. Correlation-function parameters for simulations.

Function	Λ_1^{-1} (fs)	Δ_1 (cm^{-1})	λ (cm^{-1})	Λ_2^{-1} (fs)	Δ_2 (cm^{-1})	T_2 (fs)	Pulse duration (fs)	Ref.
Fig. 6(a)	⋯	⋯	⋯	⋯	⋯	43	⋯	Figs. 1–3
Fig. 6(b)	130	471	⋯	900	408	⋯	70	24
Fig. 6(c)	500	634	37	⋯	⋯	322	200	21
Fig. 6(d)	700	54	⋯	15 000	38	90	130	23
Fig. 6(e)	36	534	⋯	463	415	⋯	δ(t)	41

work. These four correlation functions represent a large range of dynamics even though these functions are meant to describe the dephasing of the OH stretch of HDO resulting from interactions with the water (i.e., largely D$_2$O) bath.

The values from the literature used in the simulations are given in Table II (frequencies are in angular units), and the results of the simulations are shown in Fig. 6. The experimental electric field shown in Fig. 6(a) was calculated using the following information: the square root of the field intensity[42] was multiplied by a sine function with carrier frequency 1.0205×10^{14} s^{-1} (matched to the pulse spectrum) and temporal phase determined from the XFROG analysis. The same carrier frequency was used in all of the pulse propagation simulations.[43] Population relaxation is treated as a mono-exponential decay in all simulations, with T_1 =650 fs for Fig. 6(c) and T_1=700 fs for Fig. 6(b), 6(d), and 6(e). The correlation function used to calculate the propagated field shown in Fig. 6(c) was determined from wavelength-dependent pump-probe experiments;[21] those of Figs. 6(b) and 6(d) were obtained from stimulated photon

echo measurements.[23,24] Figure 6(e) shows the propagated field obtained using $C(\tau)$ from molecular dynamics (MD) simulations;[41] the propagated field of Fig. 6(f) was obtained using the correlation function from three-pulse photon-echo peak shift experiments.[22]

Clearly the different correlation functions yield very different simulated fields. Given the parameters obtained from the correlation functions, Δ_i has a strong impact on the resultant field shapes; for a given value of Λ_i, it serves to tune the dephasing dynamics along the homogeneous-inhomogeneous continuum ($\Lambda_i/\Delta_i \ll 1$ is inhomogeneous and $\Lambda_i/\Delta_i \gg 1$ is homogeneous).[1] Simulated pulse profiles were found to agree with our pulse propagation measurement in the case of modest inhomogeneous broadening. Greater inhomogeneity of the medium increases the interference among the emitters excited by coherent radiation and hence there is less coherence in the ensemble FID resulting in a rapid decrease of the coherence. Conversely one obtains prolonged FID beats in the homogeneous regime as observed in Fig. 6(e). Clearly, the linear pulse propagation measurement and application of the CF-FDTD approach can distinguish amongst correlation functions, and we suggest, provides a necessary condition to be satisfied in their determination.

V. DISCUSSION

The propagated fields presented in Refs. 13 and 20 already demonstrated the sensitivity of the time-domain fields to the details of the correlation-function shape described by a single Kubo function.[13,20] In Ref. 13, spectra obtained from the propagated fields were compared with the Fourier transform of $\exp[-g(t)]$, $\int_{-\infty}^{\infty} dt \exp[i(\omega - \omega_0)t - g(t)]$, where $g(t)$ was matched to that used in the simulation; this quantity represents the linear absorption line shape.[1] The author found that agreement between analytical and simulated spectra depends on the response further illustrating the correlation-function dependence of the propagated fields.[13] For the HDO/D$_2$O system discussed here, as the extent of inhomogeneity in the system increases, the spectrum of the propagated field better reproduces that predicted by Fourier transformation of $g(t)$ (not shown). This trend is mirrored in the response function results of Fig. 6.

The calculations reported herein focus on the response of the two-level absorbers in resonance with the incoming pulse. However, the D$_2$O solvent can also influence the resulting field profiles through nonresonant material dispersion effects. This was observed in the experimental pulse propagation measurements, which showed significant broadening of the pulse (increase in duration of $\sim$10 fs) after traveling
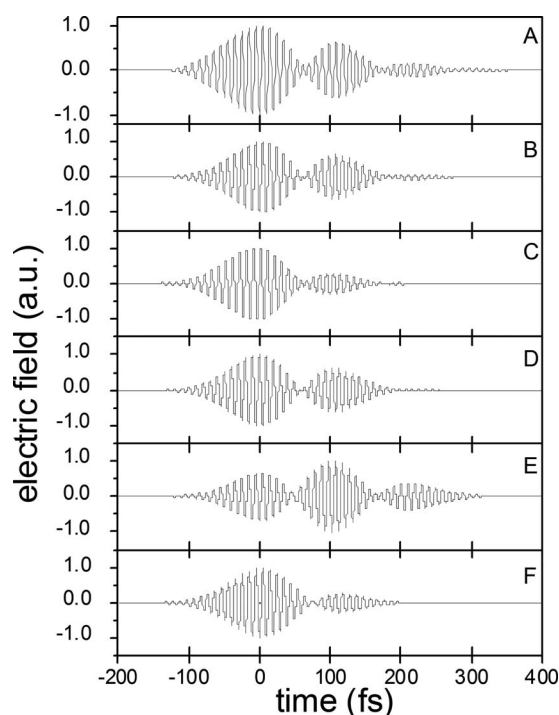

FIG. 6. Comparison between experimentally determined fields and simulations performed with correlation functions taken from the literature. (a) Experiment; (b) Yeremenko *et al.* (Ref. 24); (c) Woutersen and Bakker (Ref. 21); (d) Stenger *et al.* (Ref. 23); (e) Piryatinski *et al.* (Ref. 41); (f) Fecko *et al.* (Ref. 22). See Table II and Appendix B for correlation-function parameters.

through the neat D_2O solvent compared to the empty sample cell. In the simulations performed here, this effect is treated in a simplistic manner, setting the permittivity to that of D_2O and "prebroadening" the pulses to what they would be after propagation through the solvent. A more rigorous treatment of the solvent response could clarify the differences between the simulated FID responses and our measured results. However, this will be a constant effect and does not account for the range of correlation functions reported for the $HDO:D_2O$ system.

Because the formulas (8.42a), (8.52a), and (8.54) in Ref. 1 relating $g(t)$ to the absorption spectrum apply for one-dimensional time-domain or frequency-domain spectroscopies, these equations do not account for applied fields with finite bandwidths. However, finite bandwidths are the key to the effect observed in the present paper. The pulses used in the experiments described in Sec. II, which contain only a few optical cycles, are similar to the linewidth of the HDO/D_2O sample. Therefore, a complete measurement of the FID-modified propagated fields requires a joint time-frequency detection scheme.

The present field-resolved measurements should be most sensitive to heterogeneity when the pulse width is not much greater than the transition line width, whereby the combined experimental and simulation approach can distinguish homogeneous from inhomogeneous broadening dynamics. By contrast, pulses with infinite bandwidth are incapable of distinguishing homogeneous from inhomogeneous line broadening.[1]

Finally, we note that the bandwidth of the linear polarization can be greater than the bandwidth of the applied field only for homogeneously broadened transitions. A conventional linear absorption (transmission) spectrum does not "see" this extra bandwidth, which is outside the window of the applied field spectrum. However, the slope of the spectral phase at the peak of the linear polarization contains information about dynamics that even occur outside the bandwidth of the applied field. We have shown that the polarization emission time is affected by such extra-bandwidth dynamics.[47]

VI. CONCLUSIONS

The full-field simulations and measurements reported herein give access to the amplitude and phase changes of the field in both the time and frequency domains. We have used XFROG and Spectral Interferometry to fully characterize pulse distortions observed during resonant pulse propagation through liquid $HDO:D_2O$ solutions that are optically dense. Deviations from steady-state values are expected to occur in pulse propagation experiments where the absorption linewidth is narrower than the laser spectral width. Since portions of the pulse energy are in spectral regions beyond the linewidth of the material, the off-resonant spectral wings can propagate a larger distance than that predicted by Beer's law for the spectral components of the field that lie within the absorption linewidth. This is a factor that contributes to the observed FID beats.

The CF-FDTD method[13] was used to simulate the reso-

nant propagation of ultrashort mid-IR pulses through optically dense samples of isotopically diluted liquid water. While the pulse propagation measurement cannot uniquely determine the full coherence decay dynamics (or correlation function) of the transition, its sensitivity to early-time dephasing dynamics allows examining the accuracy of published correlation functions. In the present paper this was done for the OH-stretch transition of HDO. The CF-FDTD simulations show that published experimental correlation functions yield very different propagated fields. Simulated pulse profiles agree with experiment in the limit of modest inhomogeneous broadening. The combined experimental/simulation approach shows how linear spectroscopy can be used to assess the differences in models obtained from nonlinear measurements.

While a simple phenomenon, the coherent propagation effects on resonant fields highlight distinctions between proposed correlation functions and reveal correlation-function-dependent spectral reshaping upon propagation. Such reshaping warrants further investigation for its potential impact on coherent spectroscopic measurements. Further examination of the early-time behavior of the lineshape function in each case provides insight into the features of the dephasing necessary for reproducing experimental propagated fields. This strategy demonstrates the synergy of linear pulse propagation spectroscopy with more complicated nonlinear (mid-IR) experiments.

The experiments described here are linear, first order measurements, and the corresponding Fourier-transform relationship between the temporal profile and the spectral interferometry data is observed (Fig. 4). Yet, we note that this linear measurement appears to have attributes of "nonlinear" experiments; it has a dependence on two variables (time and frequency) and exhibits sensitivity to dephasing dynamics. Conventional linear optical experiments involve a single variable—either a (fixed) delay time or a single frequency—and correspond to one-dimensional measurements. Such single variable linear experiments result in a lineshape that cannot differentiate fast fluctuations of the transition frequencies (homogeneous line broadening) from static offsets of these transition frequencies (inhomogeneous broadening). In contrast, two-dimensional measurements, such as a two time delay Raman (or IR) experiment, are capable of unraveling details of broadened vibrational line shapes.[10,12,44] The field-resolved linear *mid-IR* measurements described in the present work may be viewed more intuitively in a joint time-frequency (spectrogram) representation. The time and frequency representations are connected by the dynamics (i.e., dephasing, depopulation) of the material response function and hence the (linear) polarization. That is, measurement of the full optical field provides the connection between the time and frequency representations through the material response function.

Finally, extension of the present experimental-Maxwell equation simulation approach may provide a route to address the issue of non-Condon effects on the (IR) spectral fluctuations of water.[45]

ACKNOWLEDGMENTS

APPENDIX A: EXTENSION OF THE CF-FDTD METHOD TO THREE-LEVEL SYSTEMS

In this extension of the CD-FDTD method, the medium is treated quantum-mechanically by evaluating the polarization term in the coupled Maxwell-Liouville equations through explicit treatment of the density matrix for a cascaded three-level system. Three-level systems are of interest to analyze, for example, the two-step excitation of a molecule through an intermediate state. The density matrix elements of the vector were chosen such that all quantities in the calculations are real. To accomplish this, the following combinations of the 3×3 (Hilbert space representation) density matrix are formed,

$$\rho_1 = \rho_{ab} + \rho_{ba},$$

$$\rho_2 = \rho_{bc} + \rho_{cb},$$

$$\rho_3 = \rho_{ac} + \rho_{ca},$$

$$\rho_4 = i(\rho_{ab} - \rho_{ba}),$$

$$\rho_5 = i(\rho_{bc} - \rho_{cb}),$$

$$\rho_6 = i(\rho_{ac} - \rho_{ca}),$$

$$\rho_7 = \rho_{bb} - \rho_{aa},$$

$$\rho_8 = [\rho_{cc} - (\rho_{aa} + \rho_{bb})], \tag{A1}$$

where a, b, and c refer to the ground state and first two excited states, respectively, of the three-level system.

The polarization of the medium is linked to the density matrix through the relation[1]

$$P_x(t) = -N\mu_{10}(\rho_{ab} + \rho_{ba}) - N\mu_{21}(\rho_{bc} + \rho_{cb})$$

$$= -N\mu_{10}\rho_1 - N\mu_{21}\rho_2, \tag{A2}$$

with N equal to the number density of three-level absorbers. Therefore, the coupled Maxwell–Liouville equations for the fields and density matrix elements are

$$\frac{\partial H_\gamma}{\partial t} = -\frac{1}{\mu_0}\frac{\partial E_x}{\partial z},$$

$$\frac{\partial E_x}{\partial t} = -\frac{1}{\varepsilon}\frac{\partial H_y}{\partial z} - \frac{1}{\mu_0}\frac{\partial P_x}{\partial t} = -\frac{1}{\varepsilon}\frac{\partial H_y}{\partial z}$$

$$-\frac{1}{\mu_0}(-N\mu_{10}\omega_{10}\rho_4 + N\mu_{10}\dot{g}(t)\rho_1$$

$$-N\mu_{12}\omega_{21}\rho_5 + N\mu_{10}\dot{g}(t)\rho_2), \tag{A3}$$

and

$$\frac{\partial \rho_1}{\partial t} = \omega_{10}\rho_4 + \frac{V_{12}}{\hbar}\rho_6 - \dot{g}(t)\rho_1,$$

$$\frac{\partial \rho_2}{\partial t} = -\omega_{12}\rho_5 - \frac{V_{12}}{\hbar}\rho_6 - \dot{g}(t)\rho_2,$$

$$\frac{\partial \rho_3}{\partial t} = \frac{V_{23}}{\hbar}\rho_4 - \frac{V_{12}}{\hbar}\rho_5 - \dot{g}(t)\rho_3,$$

$$\frac{\partial \rho_4}{\partial t} = -\omega_{10}\rho_1 + 2\frac{V_{12}}{\hbar}\rho_7 - \frac{V_{23}}{\hbar}\rho_3 - \dot{g}(t)\rho_4,$$

$$\frac{\partial \rho_5}{\partial t} = -\omega_{21}\rho_2 + \frac{V_{12}}{\hbar}\rho_3 + \frac{V_{23}}{\hbar}\sqrt{3}\rho_8 - \frac{V_{23}}{\hbar}\rho_7 - \dot{g}(t)\rho_5,$$

$$\frac{\partial \rho_6}{\partial t} = \frac{V_{12}}{\hbar}\rho_2 - \frac{V_{23}}{\hbar}\rho_1 - \dot{g}(t)\rho_6,$$

$$\frac{\partial \rho_7}{\partial t} = -2\frac{V_{12}}{\hbar}\rho_4 + \frac{V_{23}}{\hbar}\rho_5 - \frac{1}{T^{10}}\rho_7,$$

$$\frac{\partial \rho_8}{\partial t} = -2\sqrt{3}\frac{V_{23}}{\hbar}\rho_5 - \frac{1}{T^{20}}\rho_8, \tag{A4}$$

with resonant frequencies ω_{ij} and $V_{ij} = -\mu_{ij}E$, where μ_{ij} is the transition dipole moment.

Equations (A3) and (A4) for the fields and density matrix elements form the basis for the CF-FDTD algorithm applied to the cascaded three-level system. Before finite differencing, the density matrix elements are recast in a reduced form for computational simplicity, as outlined in Ref. 13. The reduced quantities are

$$\rho_i(z,t) = u_i(z,t)e^{-g(t)}, \quad i = 1\cdots6,$$

$$\rho_7(z,t) = \rho_{70} + u_7(z,t)e^{-t/T_1^{10}},$$

$$\rho_8(z,t) = \rho_{80} + u_8(z,t)e^{-t/T_1^{20}}, \tag{A5}$$

where the initial inversions for levels $b(\rho_{70})$ and $c(\rho_{80})$ have also been included.

The equations are finite differenced and tested according to standard prescriptions.[31,32] The resulting finite-differenced equations are

$$H_y\left(m + \tfrac{1}{2}, n + \tfrac{1}{2}\right) = H_y\left(m + \tfrac{1}{2}, n - \tfrac{1}{2}\right) - \frac{\Delta t}{\mu_0\Delta z}[E_x(m+1,n) - E_x(m,n)], \tag{A6}$$

$$E_x(m+1,n) = E_x(m,n) - \frac{\Delta t}{\varepsilon \Delta z}\left[H_y\left(m+\tfrac{1}{2},n+\tfrac{1}{2}\right) - H_y\left(m-\tfrac{1}{2},n+\tfrac{1}{2}\right)\right] - \Delta t A\left(n+\tfrac{1}{2}\right)\tfrac{1}{2}[u_4(m,n+1) + u_4(m,n)]$$

$$+ \Delta t C\left(n+\tfrac{1}{2}\right)\tfrac{1}{2}[u_5(m,n+1) + u_5(m,n)] - \Delta t D\left(n+\tfrac{1}{2}\right)\tfrac{1}{2}[u_1(m,n+1) + u_1(m,n)], \tag{A7}$$

$$u_1(m,n+1) = u_1(m,n) + \Delta t \omega_{01}\tfrac{1}{2}[u_4(m,n+1) + u_4(m,n)] + \frac{\mu_{12}}{\hbar}\Delta t \tfrac{1}{2}[u_6(m,n+1) + u_6(m,n)]\tfrac{1}{2}[E_x(m+1,n) + E_x(m,n)] \tag{A8}$$

$$u_2(m,n+1) = u_1(m,n) + \Delta t \omega_{12}\tfrac{1}{2}[u_5(m,n+1) + u_5(m,n)] - \frac{\mu_{01}}{\hbar}\Delta t \tfrac{1}{2}[u_6(m,n+1) + u_6(m,n)]\tfrac{1}{2}[E_x(m+1,n) + E_x(m,n)], \tag{A9}$$

$$u_3(m,n+1) = u_3(m,n) + \frac{\mu_{12}}{\hbar} . \Delta t . \tfrac{1}{2} . [u_4(m,n+1) + u_4(m,n)] . \tfrac{1}{2} . [E_x(m+1,n) + E_x(m,n)]$$

$$- \frac{\mu_{01}}{\hbar} . \Delta t . \tfrac{1}{2} . [u_5(m,n+1) + u_5(m,n)] . \tfrac{1}{2} . [E_x(m+1,n) + E_x(m,n)], \tag{A10}$$

$$u_4(m,n+1) = u_4(m,n) - \Delta t . \omega_{01} . \tfrac{1}{2} . [u_1(m,n+1) + u_1(m,n)] - \frac{2\mu_{12}}{\hbar} . \Delta t . \tfrac{1}{2} . [u_3(m,n+1) + u_3(m,n)] . \tfrac{1}{2} . [E_x(m+1,n)$$

$$+ E_x(m,n)] + G\left(n+\tfrac{1}{2}\right) . \tfrac{1}{2}[E_x(m+1,n) + E_x(m,n)] + I_+\left(n+\tfrac{1}{2}\right) . \Delta t . \tfrac{1}{2}[u_7(m,n+1) + u_7(m,n)] . \tfrac{1}{2} . [E_x(m$$

$$+ 1,n) + E_x(m,n)], \tag{A11}$$

$$u_5(m,n+1) = u_5(m,n) - \Delta t . \omega_{12} . \tfrac{1}{2} . [u_2(m,n+1) + u_2(m,n)] + \frac{\mu_{01}}{\hbar} . \Delta t . \tfrac{1}{2}[u_3(m,n+1) + u_3(m,n)] . \tfrac{1}{2} . [E_x(m+1,n)$$

$$+ E_x(m,n)] - G^a\left(n+\tfrac{1}{2}\right) . \tfrac{1}{2} . [E_x(m+1,n) + E_x(m,n)] - I_+^\sigma\left(n+\tfrac{1}{2}\right) . \Delta t . \tfrac{1}{2}[u_7(m,n+1) + u_7(m,n)] . \tfrac{1}{2} . [E_x(m$$

$$+ 1,n) + E_x(m,n)] + J\left(n+\tfrac{1}{2}\right) . \tfrac{1}{2} . [E_x(m+1,n) + E_x(m,n)], \tag{A12}$$

$$u_6(m,n+1) = u_6(m,n) - \frac{\mu_{12}}{\hbar} . \Delta t . \tfrac{1}{2} . [u_1(m,n+1) + u_1(m,n)] . \tfrac{1}{2} . [E_x(m+1,n) + E_x(m,n)]$$

$$+ \frac{\mu_{01}}{\hbar} . \Delta t . \tfrac{1}{2} . [u_2(m,n+1) + u_2(m,n+1)] . \tfrac{1}{2} . [E_x(m+1,n) + E_x(m,n)], \tag{A13}$$

$$u_7(m,n+1) = u_7(m,n) - I_-\left(n+\tfrac{1}{2}\right)\Delta t \tfrac{1}{2}[u_4(m,n+1) + u_4(m,n)]\tfrac{1}{2}[E_x(m+1,n) + E_x(m,n)]$$

$$+ I_-^a\left(n+\tfrac{1}{2}\right)\Delta t \tfrac{1}{2}[u_5(m,n+1) + u_5(m,n)]\tfrac{1}{2}[E_x(m+1,n) + E_x(m,n)], \tag{A14}$$

$$u_8(m,n+1) = u_8(m,n) - K_-\left(n+\tfrac{1}{2}\right)\Delta t \tfrac{1}{2}[u_5(m,n+1) + u_5(m,n)]\tfrac{1}{2}[E_x(m+1,n) + E_x(m,n)], \tag{A15}$$

where m and n are the space and time step locations, respectively. The time-dependent coefficient in Eqs. (A7)–(A15) are defined as

$$A(t) \equiv \frac{N\mu_{01} . \omega_{01} . e^{-g(t)}}{\varepsilon},$$

$$C(t) \equiv \frac{N\mu_{12} . (-\omega_{12}) . e^{-g(t)}}{\varepsilon},$$

$$D(t) \equiv \frac{N\mu_{01} . \dot{g}(t) . e^{-g(t)}}{\varepsilon},$$

$$G(t) \equiv \frac{2\mu_{01}}{\hbar} . \rho_{70} . e^{+g(t)},$$

$$G^a(t) \equiv \frac{\mu_{12}}{\hbar} . \rho_{70} . e^{+g(t)},$$

$$I_+(t) \equiv \frac{2\mu_{01}}{\hbar} . e^{+g(t)} . e^{-t/T_1^{10}},$$

$$I_-(t) \equiv \frac{2\mu_{01}}{\hbar} . e^{-g(t)} . e^{+t/T_1^{10}},$$

$$I_+^a(t) \equiv \frac{\mu_{12}}{\hbar} \cdot e^{+g(t)} \cdot e^{-t/T_1^{10}},$$

$$I_-^a(t) \equiv \frac{\mu_{12}}{\hbar} \cdot e^{-g(t)} \cdot e^{+t/T_1^{10}},$$

$$J^a(t) \equiv \sqrt{3} \cdot \frac{\mu_{12}}{\hbar} \cdot \rho_{80} \cdot e^{+g(t)},$$

$$K_-(t) \equiv \sqrt{3} \cdot \frac{\mu_{12}}{\hbar} \cdot e^{-g(t)} \cdot e^{+t/T_1^{20}}.$$

The details of the FDTD time propagation and use of the differenced equations is analogous to the description in Ref. 13. The finite-differenced time-dependent coefficients are obtained by making the substitution $t = n + 1/2$.

APPENDIX B: LINE SHAPE FUNCTION DERIVED FROM $C(\tau)$ OF REFERENCE 22

The correlation function from Ref. 22 was constructed assuming two overdamped and two underdamped Brownian oscillators,

$$C(\tau) = \sum_{n=1}^{A} A_n \left\{ e^{-\gamma_n \tau} \left[\cos(\omega_n \tau) + \frac{\gamma_n}{\omega_n} \sin(\omega_n \tau) \right] \right\}. \quad (B1)$$

The fit parameters, taken from Table II of Ref. 22, are $A_1 = 2.05 \times 10^{-4}$ fs^{-2}, $A_2 = 1.03 \times 10^{-4}$ fs^{-2}; $A_3 = 2.47 \times 10^{-4}$ fs^{-2}; $A_4 = 2.82 \times 10^{-5}$ fs^{-2}; $1/\gamma_1 = 107$ fs; $1/\gamma_2 = 1410$ fs; $1/\gamma_3 = 104$ fs; $1/\gamma_4 = 40$ fs; $\omega_3/2\pi = 175$ cm^{-1}; $\omega_4/2\pi = 400$ cm^{-1}.

The line shape function, $g(t) = \int_0^t d\tau_2 \int_0^{\tau_2} d\tau_1 C(\tau_1)$, associated with the particular form of Eq. (B1) given in Ref. 22 is

$$
\begin{aligned}
g(t) = &\sum_{n=1}^{2} \left[A_n(1 + t\gamma_n \exp(\gamma_n \tau)) \frac{\exp(-\gamma_n t)}{\gamma_n^2} - \frac{A_n}{\gamma_n^2} \right] \\
&+ \sum_{n=3}^{4} \left\{ \frac{A_n \exp(-\gamma_n t)}{(\gamma_n^2 + \omega_n^2)^2 \omega_n} [3\omega_n \gamma_n^2 \cos(\omega_n t) \right. \\
&- 3\omega_n^2 \gamma_n \sin(\omega_n t) - \omega_n^3 \cos(\omega_n t) + \gamma_n^3 \sin(\omega_n t) \\
&+ 2\gamma_n^2 \omega_n \exp(\gamma_n t) + 2\gamma_n \omega_n^3 t \exp(\gamma_n t)] \\
&\left. - A_n(3\gamma_n^2 - \omega_n^2)/(\gamma_n^2 + \omega_n^2)^2 \right\}. \quad (B2)
\end{aligned}
$$

[1] S. Mukamel, *Principles of Nonlinear Optical Spectroscopy* (Oxford University Press, New York, 1995).

[2] M. H. Cho, N. F. Scherer, G. R. Fleming, and S. Mukamel, J. Chem. Phys. **96**, 5618 (1992).

[3] M. S. Pshenichnikov, W. P. de Boeij, and D. A. Wiersma, Phys. Rev. Lett. **76**, 4701 (1995).

[4] M. K. Yetzbacher, N. Belabas, K. A. Kitney, and D. M. Jonas, J. Chem. Phys. **126**, 044511 (2007).

[5] D. M. Jonas, Annu. Rev. Phys. Chem. **54**, 425 (2003).

[6] D. Zigmantas, E. L. Read, T. Mancal, T. Brixner, A. T. Gardiner, R. J. Cogdell, and G. R. Fleming, Proc. Natl. Acad. Sci. U.S.A. **103**, 12672 (2006).

[7] D. W. McCamant, P. Kukura, S. Yoon, and R. A. Matthies, Rev. Sci. Instrum. **75**, 4971 (2004).

[8] A. M. Moran, R. A. Nome, and N. F. Scherer, J. Chem. Phys. **125**, 031101 (2006).

[9] V. Wong and I. A. Walmsley, Opt. Lett. **19**, 287 (1994).

[10] M. C. Asplund, M. T. Zanni, and R. M. Hochstrasser, Proc. Natl. Acad. Sci. U.S.A. **97**, 8219 (2000).

[11] M. Khalil, N. Demirdoven, and A. Tokmakoff, J. Phys. Chem. A **107**, 5258 (2003).

[12] J. B. Asbury, T. Steinel, C. Stromberg, K. J. Gaffney, I. R. Piletic, A. Goun, and M. D. Fayer, Phys. Rev. Lett. **91**, 237402 (2003).

[13] J. A. Gruetzmacher, J. Chem. Phys. **119**, 1590 (2003).

[14] R. G. Brewer and R. L. Shoemaker, Phys. Rev. A **6**, 2001 (1972).

[15] J. E. Rothenberg, D. Grischkowsky, and A. C. Balant, Phys. Rev. Lett. **53**, 552 (1984).

[16] H. J. Hartmann and A. Laubereau, Opt. Commun. **47**, 117 (1983).

[17] K. E. Oughstun, *Electromagnetic and Optical Pulse Propagation I: Spectral Representation in Temporally Dispersive Media* (Springer-Verloag, New York, 2006).

[18] C. G. B. Garrett and D. E. Mccumber, Phys. Rev. A **1**, 305 (1970).

[19] R. Trebino, *Frequency Resolved Optical Gating: The Measurement of Ultrashort Laser Pulses* (Kluwer, Boston, 2000).

[20] J. A. Gruetzmacher and N. F. Scherer, Opt. Lett. **28**, 573 (2003).

[21] S. Woutersen and H. J. Bakker, Phys. Rev. Lett. **83**, 2077 (1999).

[22] C. J. Fecko, J. J. Loparo, S. T. Roberts, and A. Tokmakoff, J. Chem. Phys. **122**, 054506 (2005).

[23] J. Stenger, D. Madsen, P. Hamm, E. T. J. Nibbering, and T. Elsaesser, J. Phys. Chem. A **106**, 2341 (2002).

[24] S. Yeremenko, M. S. Pshenichnikov, and D. A. Wiersma, Chem. Phys. Lett. **369**, 107 (2003).

[25] R. A. Nome, Ph.D. thesis, University of Chicago, 2007.

[26] S. Woutersen and H. J. Bakker, Nature (London) **402**, 507 (1999).

[27] S. Linden, H. Giessen, and J. Kuhl, Phys. Status Solidi B **206**, 119 (1998).

[28] J. A. Gruetzmacher and N. F. Scherer, Rev. Sci. Instrum. **73**, 2227 (2002).

[29] J. A. Gruetzmacher and N. F. Scherer, in *Ultrafast Phenomena XII*, edited by T. Elsasser, S. Mukamel, M. M. Murnane, and N. F. Scherer (Springer-Verlag, Berlin, 2000), pp. 530–532.

[30] A. Yabushita, T. Fuji, and T. Kobayashi, Opt. Commun. **198**, 227 (2001).

[31] A. Taflove and S. C. Hagness, *Computational Electrodynamics: The Finite-Difference Time-Domain Method*, 2nd ed. (Artech House, Inc., Norwood, MA, 2000).

[32] R. J. Luebbers and K. S. Kunz, *The Finite Difference Time Domain Method for Electromagnetics* (CRC, Boca Raton, FL, 1993).

[33] H. R. Wyss and M. Falk, Can. J. Chem. **48**, 607 (1970).

[34] J. E. Bertie, M. Khalique Ahmed, and H. H. Eysel, J. Phys. Chem. **93**, 2210 (1989).

[35] D. C. Burnham and R. Y. Chiao, Phys. Rev. **188**, 667 (1969).

[36] A. Laubereau and W. Kaiser, Rev. Mod. Phys. **50**, 607 (1978).

[37] S. M. Gallagher, A. W. Albrecht, T. D. Hybl, B. L. Landin, B. Rajaram, and D. M. Jonas, J. Opt. Soc. Am. B **15**, 2338 (1998).

[38] L. Lepetit, G. Cheriaux, and M. Joffre, J. Opt. Soc. Am. B **12**, 2467 (1995).

[39] E. Tokunaga, A. Terasaki, and T. Kobayashi, J. Opt. Soc. Am. B **12**, 753 (1995).

[40] L. Allen and J. H. Eberly, *Optical Resonance and Two-Level Atoms* (Dover, New York, 1987).

[41] A. Piryatinski, C. P. Lawrence, and J. L. Skinner, J. Chem. Phys. **118**, 9664 (2003).

[42] Here, the field "intensity" refers to the square of the field envelope. The term "amplitude" denotes the magnitude of the field envelope itself.

[43] As in all FROG methods, the phase is only determined to within a constant, additive factor. However, the inability of the FROG algorithm to determine an "absolute" phase does not impact the phase jumps and any residual chirp on the pulses which determine the details of the waveform, especially in the nodal regions. The pulse spectral content is used to set the carrier frequency in all cases.

[44] Y. Tanimura and S. Mukamel, J. Chem. Phys. **99**, 9496 (1993).

[45] J. R. Schmidt, S. A. Corcelli, and J. L. Skinner, J. Chem. Phys. **123**, 044513 (2005).

[46] A. A. Ferro, J. D. Hybl, and D. M. Jonas, J. Chem. Phys. **114**, 4649 (2001).

[47] A. M. Moran, S. Park, and N. F. Scherer, J. Phys. Chem. B **110**, 19771 (2006).